Available online at www.sciencedirect.com
ScienceDirect
Cement & Concrete Composites 29 (2007) 677–689
Cement & Concrete Composites
www.elsevier.com/locate/cemconcomp

Effect of surface pre-conditioning on bond of carbon fibre reinforced polymer rods to concrete

Firas AL-mahmoud [a,*], Arnaud Castel [a], Raoul François [a], Christian Tourneur [b]

[a] L.M.D.C. INSA-UPS, 135 Avenue de Rangueil, 31077 Toulouse Cedex 4, France
[b] Freyssinet. 11, Avenue du 1er Mai, 91127 Palaiseau Cedex, France

Received 7 February 2006; received in revised form 19 March 2007; accepted 12 April 2007
Available online 29 April 2007

Abstract

The experimental program developed in this work aims at investigating the possibility of using carbon fibre reinforced polymer rods to strengthen concrete structural members. Firstly, physical, chemical and mechanical tests were performed on carbon fibre reinforced polymer. Secondly, the bond between carbon fibre reinforced polymer rod and concrete was studied by using the pull-out test. Different types of surface treatment were applied to the smooth rods in order to enhance the bond with concrete. Firstly, the rods were machined using a lathe and a grinding stone to create lugs with different configurations. Secondly, the rods were coated with sand of various grain sizes. The sand was fixed on the rods with a thin layer of epoxy resin.

The experimental results indicate that carbon fibre reinforced polymer rod seems to be a good option for strengthening concrete structural members. Results showed a very good physical, chemical and mechanical compatibility between the rods and the concrete. Depending on the surface treatment process, the ultimate bond strength can reach twice that of ribbed steel bars. Moreover, the residual friction between the carbon fibre reinforced polymer rods and the concrete (softening branch) remained equivalent to or greater than that of ribbed steel bar.

Keywords: CFRP; Rod; Strengthening; Bond strength; Surface treatment

1. Introduction

The need to rehabilitate civil structures is becoming a serious problem for building owners. The first traditional techniques for strengthening reinforced concrete structures use steel plates or post-tensioned cables bonded in the tension regions [1–3]. The limitations of such methods stem from the high additional weight imposed on the structure and the dubious durability of the strengthening due to corrosion or other environmental attacks. An option to overcome the above-mentioned problems is the fiber-reinforced polymer (FRP) composite material. One of the methods available to implement FRP materials in concrete structures is the near-surface mounted (NSM) technique, where composite rods are bonded in a pre-sawn groove in the concrete cover. This technique has attracted extensive research in recent years [4–9].

The main advantages to use fiber-reinforced polymer composite are a high tension strength for a low density, absence of sensitivity to corrosion and a long fatigue life [10–14]. Their low density reduces the installation cost and their high strength in tension, which can reach 10 times that of the usual reinforcing steel, limits the cross-sections. All these factors offset the high cost of these materials. However, several problems still remain to be solved, such as the anisotropy and variability of the physical properties compared to usual steel products [15], the low ductility of

* Corresponding author. Tel.: +33 561 559 933; fax: +33 561 559 949.
E-mail addresses: firas@insa-toulouse.fr (F. AL-mahmoud), castel@insa-toulouse.fr (A. Castel), francois@insa-toulouse.fr (R. François), ctourneur@freyssinet.com (C. Tourneur).

0958-9465/$ - see front matter © 2007 Elsevier Ltd. All rights reserved.
doi:10.1016/j.cemconcomp.2007.04.010

the materials [16], their bond with concrete [17–24], and a certain lack of knowledge due to the relatively recent development of the method.

The composite material used in this study is a carbon-epoxy pultruded fiber-reinforced polymer smooth rod 12 mm in diameter made by Soficar Company in France. The ultimate goal is to use these carbon fiber reinforced polymer (CFRP) rods to strengthen concrete structures by applying the NSM technique. In this study, a preliminary work is carried out. Firstly, physical, chemical and mechanical tests were performed in order to characterize the CFRP and analyze its compatibility with the concrete (analysis of hydrates at the interface and water absorption). Secondly, pull-out tests were performed to investigate the bond between the CFRP rod and concrete. Indeed, in spite that for NSM technique, rods are usually bonded in a filling material (resin or mortar), it seemed necessary to firstly compare the bond properties of CFRP rods and ordinary reinforcing steel bars to concrete.

Recent studies have shown that, generally, the bond between the concrete and smooth FRP rods is affected by the non-isotropic mechanical properties of the FRP. The mechanical properties in the longitudinal direction are controlled by the fibres, but in the transversal direction, the stiffness and the strength depend on the resin matrix, the low elastic modulus of which can reduce the bond strength [17]. Moreover the relative smoothness of FRP rods in the longitudinal direction compared to steel reinforcing bars can also reduce the friction and thus the bond strength with the concrete. Other researchers have shown that both the temperature increase resulting from concrete hydration and water absorption lead to swelling of the FRP rods [19,22]. The bond with the concrete is mainly dependent on the resulting radial pressures in the case of smooth FRP rods [14,23]. The additional pressure due to concrete shrinkage is also an important parameter. To conclude, the bond between smooth FRP rods and concrete is a complex problem which depends greatly on the physical and chemical properties of the composite materials, especially the matrix resin and its compatibility with the concrete in terms of porosity, thermal swelling, elastic modulus, and chemical reactivity.

In this study, bond between smooth CFRP rods and smooth ordinary steel bars to concrete were compared. But in order to limit the drawbacks just mentioned, different types of surface treatment were also applied to the smooth CFRP rods. In this case, bond strength of the usual steel ribbed bar was used as the reference.

2. Materials

One type of FRP rod was used: carbon-epoxy pultruded FRP with a diameter of 12 mm. This rod is made by the Soficar Company in France. The elastic modulus and tension strength of the CFRP rods were determined by laboratory testing.

To modify the surface configurations of the initially smooth rods, two different surface treatments were applied:

(1) *Surface machining:* a turning lathe and a grinding stone were used to create lugs on the CFRP rods. The three configurations tested are presented in Fig. 1. The dimensions of the lugs for the three configurations are given in Fig. 2.
(2) *Surface sanding:* the smooth CFRP rods were coated with three types of sand 1, 2 and 3 of various grain sizes ranging from 0.1 to 0.2, 0.2 to 0.3, and 0.3 to 0.4 mm granulometry, respectively, by sprinkling the sand onto a thin layer of freshly applied Eponal epoxy resin made by Bostik Findey Company, Fig. 1. This method was developed by the Freyssinet Company.

Three vibrated concretes (VC) were studied. Their compositions are given in Table 1.

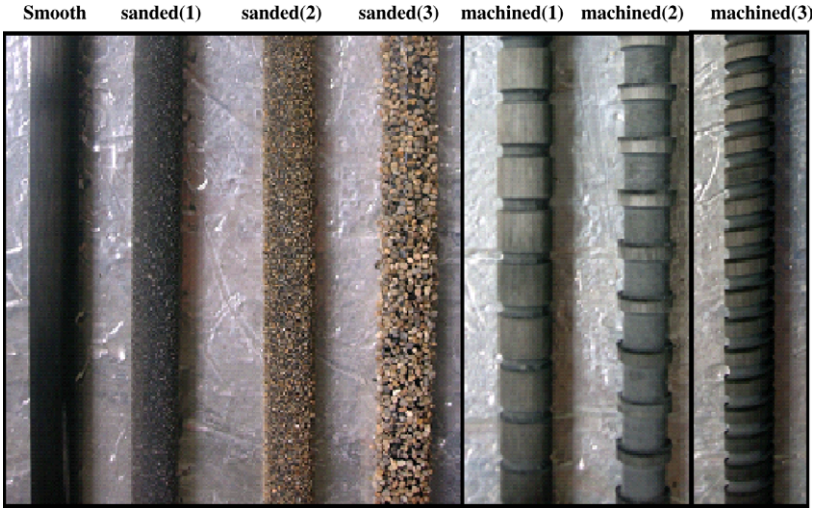

Fig. 1. Sanded and machined CFRP rods used in the study.

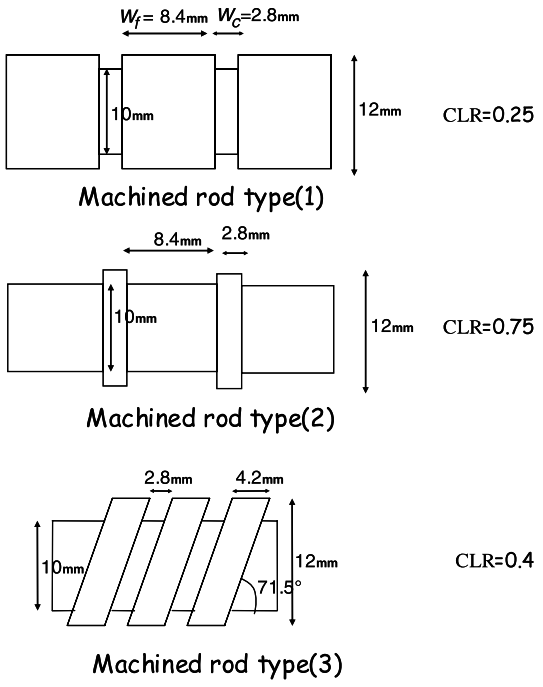

$$\textit{Concrete Lugs Ratio}\ (\mathrm{CLR}) = \frac{\textit{concrete width}}{(\textit{concrete} + \textit{CFRP})\ \textit{width}} = \frac{w_c}{w_c + w_f}$$

Fig. 2. Lug dimensions for three types of machined CFRP rods.

Table 1
Composition of the vibrated concretes

	VC30 (kg/m^3)	VC40 (kg/m^3)	VC60 (kg/m^3)
Cement CEM I 52.5 N CE CP2 NF from Gargenville calcia	280	400	390
Sand 0/4 SC NF Sandrancourt	768	710	750
Rolled gravel 4/10	324	532.5	400
Crushed gravel 10/14	839	532.5	730
Superplasticizer			10.91
Total water	176	185	145

The properties of the hardened concrete (compressive strength, tension strength and instantaneous elastic modulus) were measured at 28 days on concrete cylinders (diameter = 110 mm, height = 220 mm). The specimens were removed from their molds 24 h after casting and stored for 28 days in a confined room ($T^0 = 20$ °C, RH% = 60%). The tension strength was obtained through splitting tests. Table 2 shows the mechanical properties obtained for the three concretes.

3. Experimental program

The aim of the experimental program was to measure some physical and mechanical properties of the CFRP rods and their interaction with concrete. The density and the porosity accessible to water were measured. Electronic microscopy observations of the cross-section of the rod were performed to assess the arrangement of the carbon fibres.

The mechanical properties measured for the rods were tension strength, elastic modulus and splitting transverse tension strength.

X-ray diffractometry tests were performed on cement paste cast on CFRP rod samples in order to analyze the chemical properties of the hydrates formed at the interface with the CFRP rods and to compare them with those obtained with steel.

Bonding of the CFRP rods with concrete was investigated (pull-out test) for the various surface treatments and the smooth initial surface.

3.1. Physical–chemical–mechanical properties of smooth CFRP

3.1.1. Determination of the density and the porosity accessible to water

The density of the rods was compared with that of steel.

The porosity accessible to water gives a measure of the possibility for water to penetrate into the CFRP rod, which can influence the degree of hydration of the cement paste (concrete) embedding the rod, and also the swelling of the rod.

These tests were performed on 1.2×6 cm specimens.

For more details on the experimental procedures, see Ref. [25].

3.1.2. Scanning electron microscope (SEM) observations

The microstructure of the cross-section of the CFRP rod was studied with a JSM JEOL 840 electron microscope equipped with an elementary analysis system using X-ray spectrometry. The purpose was to characterize the cross-section of the rod in term of the percentage of fibres and to evaluate the effective perimeter in comparison to the nominal perimeter.

3.1.3. Splitting tests

These tests were performed on cylindrical specimens of 1.2×5.4 cm. The purpose was to compare the transverse

Table 2
Mechanical properties of the concretes, SD: standard deviation

Concretes	Compressive strength/SD (MPa)	Number of samples	Tension strength/SD (MPa)	Number of samples	Elastic modulus/SD (GPa)	Number of samples
VC30	34.0/2.2	3	2.6/0.2	3	32.2/1.1	3
VC40	45.6/1.7	3	3.6/0.2	3	38.1/2.5	3
VC60	65.7/2.9	3	5.4/0.3	3	43.4/2.6	3

tension strength of CFRP rods with the axial tension strength in order to reveal the degree of anisotropy of the material.

Splitting tests were carried out using a hydraulic loading machine having a capacity of 200 kN (±1.3‰ precision). The specimen was placed on a rectangular support and a compression force was then applied at a constant specification loading rate of 0.1 kN/s until the specimen failed.

The splitting tension strength was calculated according to relation:

$$\sigma_u = \frac{2F_{\max}}{\pi \cdot \phi \cdot L} \quad (1)$$

where σ_u is the splitting tension strength (MPa), ϕ is the rod diameter (mm), L is the length of the sample (mm) and $F_{\max}$ is the ultimate load (N).

3.1.4. Tension strength and elastic modulus tests

Each of the three specimens was cut into 100-cm long sections. The CFRP rod was bonded to steel cylinders at each end with epoxy resin. The tests consisted of recording the applied load by a hydraulic loading machine having a capacity of 200 kN (±1.3‰ precision) and the value of strains at the middle of the CFRP rod using 30-mm-long strain gauges glued symmetrically on either side of each rod. Thus, the strain used to calculate the tension strength and the elastic modulus corresponded to the average value. The load was applied at a constant rate of 0.1 kN/s until the specimen failed.

3.1.5. X-ray diffractometry on the cement paste (DRX)

A cement paste was cast on a piece of CFRP cut longitudinally in order to create the flat surface required for DRX measurement. The cement paste was in contact with the fibres as well as the epoxy surface of the CFRP rods. The cement paste at the interface with the CFRP was tested at 2, 7, 14 and 28 days. The same test was also performed using a steel bar.

The X-ray diffraction tests were carried out using a D5000 diffractometer. The analyses were made within an angle of 2θ ranging from 4° to 70° with a step of 0.03 and a counting time of 6 s. The purpose was to compare the hydration sequences of a cement paste in contact with the CFRP rods and another in contact with steel as these could influence the properties of the bond with the concrete. Electron microscope observations were also performed of the hydrate at the interface.

3.2. CFRP-concrete bond test

The purpose of the pull-out tests was to investigate the anchoring capacity of the rods in the concrete and the effects of different parameters, such as the surface state (smooth, machined, or sanded), on the bond characteristics of the CFRP rods.

The pull-out behavior of CFRP rods anchored in the concrete was expressed by load–slip curves, characterized by the maximum and residual bond stress, and initial stiffness of the anchors. The usual pull-out tests were carried out as shown in Fig. 3. The experimental set up was similar to the pull-out test described in the RILEM recommendation [26]. Tests were performed by using the same loading machine as the one used to measure the tension strength of the CFRP rods (Section 3.1.4) with a loading rate of 0.1 kN/s. Slip was measured through an LVDT located at the free end of the bar. The ultimate bond strength was calculated from relation:

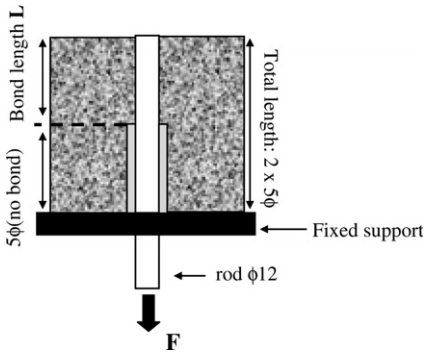

Fig. 3. Pull-out test according to RILEM recommendation.

$$\tau_u = \frac{F_{\max}}{\pi \cdot \phi \cdot L} \quad (2)$$

where τ_u is the ultimate bond strength (MPa), ϕ is the rod diameter (mm), L is the bond length (mm) and $F_{\max}$ is the ultimate load (N).

For all tests, specimens had a square cross-section of $100 \times 100\ mm^2$. For the members reinforced by the CFRP rods, the pull-out tests were carried out with both 5∅ and 10∅ bond lengths. Concerning the members reinforced by steel, the pull-out tests were only carried out with 5∅ bond length. Two different types of steel bars were used: 12-mm-diameter smooth bars and 12-mm diameter ribbed bars (yield strength = 500 MPa).

4. Results and discussion

4.1. Physical–chemical–mechanical properties of CFRP rods

4.1.1. Electron microscopy (SEM) observations

Fig. 4A shows an SEM observation of a transverse cross-section of CFRP rods. The CFRP rod is composed of fibres of carbon assembled with an epoxy matrix. Image analysis gave the ratio of the epoxy matrix as approximately 25% (±2%) of the cross-section.

Fig. 4B is a picture of the surface of the CFRP rod after the separation from the cement paste after 28 days. This figure shows that there are some zones where the cement paste persists, especially in the void between the fibres that constitute the exterior surface of the CFRP rod. The roughness of carbon fibres is almost zero. The effective surface area per unit length of CFRP rod was about 1.4 times

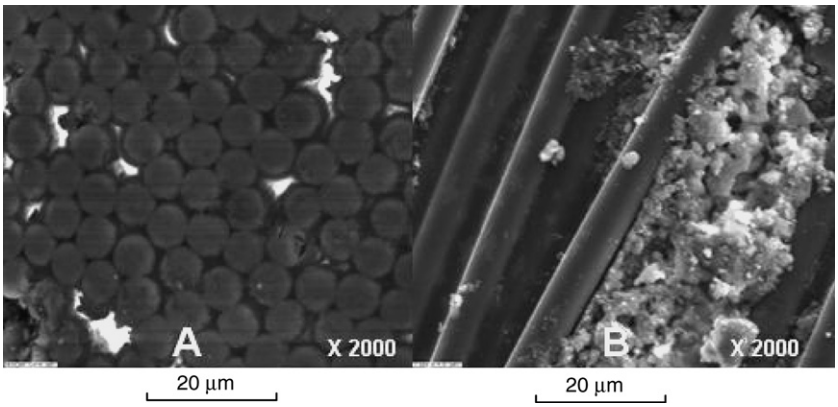

Fig. 4. (A) Transverse cross-section of CFRP rods, and (B) surface of the CFRP rod after the separation of the cement paste.

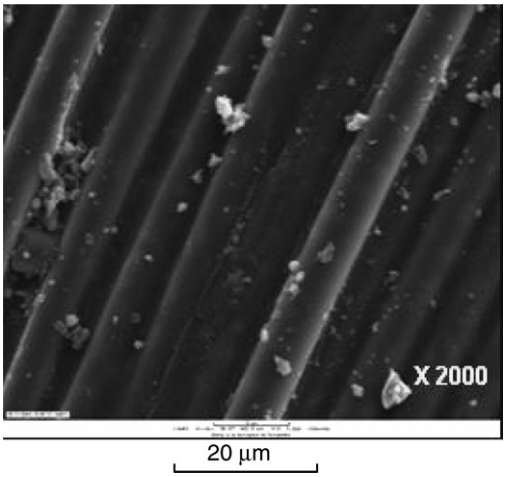

Fig. 5. Outer surface of smooth CFRP rod.

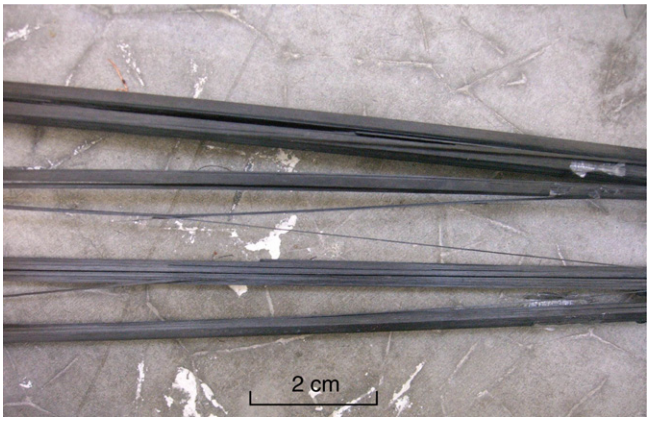

Fig. 6. Failure mode of the CFRP rod in tension.

the calculated perimeter because of the fibres which composed its outer surface as seen in Fig. 5.

4.1.2. Density and the porosity accessible to water

Table 3 shows the average values obtained on four samples. As expected, the CFRP rod was not porous to water.

4.1.3. Splitting tests

Table 3 shows the results obtained on eight samples. The splitting strength is about 1/100 of the tension strength obtained by an axial test. This shows the anisotropic properties of CFRP rods. All specimens failed by epoxy matrix failure in which a crack propagated through the epoxy matrix.

4.1.4. Tension strength test and elastic modulus tests

Fig. 6 shows the failure mode of a smooth CFRP rod tested in axial tension. The three specimens brittle failure started with splitting and ended with rupture of the rod. The rods split into different numbers and sizes of pieces. As shown in Fig. 7, a typical stress–strain curve of CFRP rods is linear up to the point of failure, and does not exhibit any yielding like that observed for steel bars. Table 3 shows the strengths and the elastic modulus test results obtained on three specimens. The elastic modulus of the CFRP rods was about 30% lower than that of steel and that their ultimate strength was about four times that of steel.

4.1.5. X-ray diffractometry of cement paste (DRX)

Fig. 8 shows the sequences of hydration of a Portland cement paste in contact with both materials (steel and CFRP) at several terms (2, 7, 14 and 28 days). The main peaks correspond to the non-hydrated or hydrated products of a Portland cement paste: C3S, C2S, C3A, C4AF, Portlandite, and Ettringite. At each term, we see that the peaks are the same for both materials (CFRP and steel),

Table 3
Apparent density, porosity accessible to water, splitting strength, strength and elastic modulus test results for the CFRP rod, SD: standard deviation

Mean apparent density/SD for 4 samples (kg/m^3)	Mean porosity accessible to the water/SD for 4 samples (%)	Mean σ_t/SD for 8 samples (MPa)	Mean elastic modulus/SD for 3 samples (GPa)	Mean strength/SD for 3 samples (MPa)
1579/6.6	0.74/0.07	24/2.1	145.9/0.6	1875/35

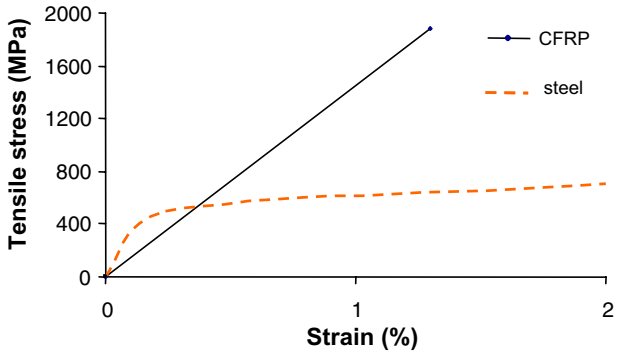

Fig. 7. Typical tension stress–strain curves of steel and CFRP rods.

which means that the hydrates formed in contact with carbon are the same as those formed in contact with steel.

4.2. CFRP-concrete bond test

4.2.1. Specimens reinforced with smooth rods

The average ultimate bond strength (τ_u) obtained on three specimens (smooth steel or CFRP), for the three types of concrete, are reported in Table 4. Fig. 9 shows the most representative bond stress (τ) versus slip (s) curves obtained for each concrete.

The value of τ_u for the smooth steel bars is always greater than that for the CFRP rods whatever the concrete strength. Therefore, the loss of adhesion with the concrete occurs earlier in the case of the CFRP rods than with the steel bars although the effective surface area per unit length of CFRP rod is about 1.4 times that based on the nominal perimeter because of the fibres which compose its outer surface (Fig. 5).

This relatively poor adhesion can be explained by the low roughness of the CFRP rods in the longitudinal direction (Fig. 5) in comparison with the roughness of the steel bars (as shown in Fig. 10). Because of the weak bonding of the smooth CFRP rods in comparison with the smooth steel bars, it is necessary to modify the surface state of the rods to enhance the bond with the concrete. The smooth CFRP rods were therefore sanded or machined and their bond properties were compared with those of the usual ribbed steel bars.

4.2.2. Specimens reinforced with machined rods

Experimental τ–s curves obtained on machined CFRP rods with 5∅ and 10∅ embedment lengths, in a VC30 concrete, are shown in Fig. 11. In this figure, only one representative curve is reported for each configuration. As shown in Fig. 12, there are two types of failure: (1) by the shearing off of the lugs of the CFRP rod (rupture of the epoxy matrix) (type 2), and (2) by the shearing off of concrete lugs (types 1 and 3).

When the rupture occurs by the shearing off of the lugs of the CFRP rod, the diameter considered to calculate the bond stress τ is 10 mm as the lugs are 1 mm in height. On the other hand, when the failure occurs by the shearing off of concrete lugs, the diameter considered is 12 mm (Fig. 12).

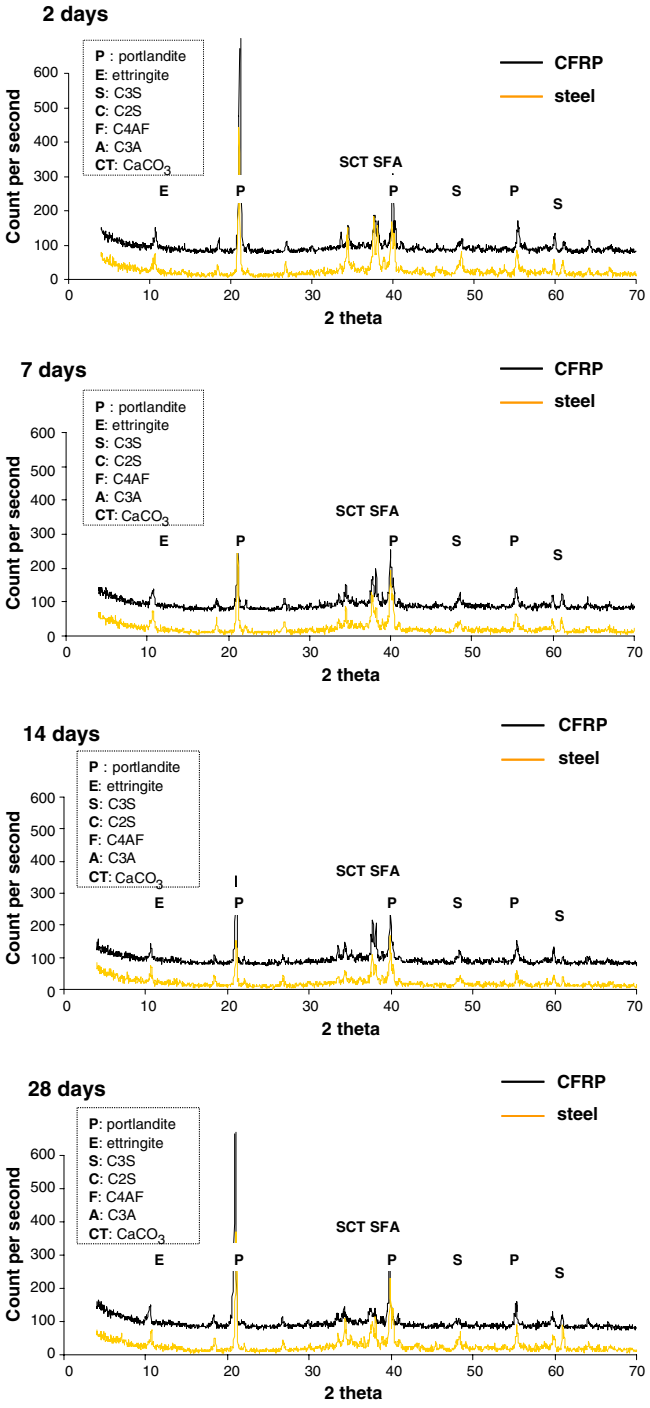

Fig. 8. X-ray diffractometry results for the cement paste.

Table 5 gives the average ultimate load and the average ultimate bond strength τ_u obtained on three specimens (in the case of 5∅ embedment length) for the three types of machined CFRP rods. The table shows that the ultimate bond strength of machined CFRP rod type 2 is higher than that of the machined CFRP rod types 1 and 3, whatever the embedment length.

Table 4
Summary of ultimate bond strength of smooth CFRP rods and smooth steel bars (bond length = 5ϕ), SD: standard deviation

Concrete strength	Material (smooth)	Number of samples	τ_u/SD (MPa)
VC30	CFRP	3	3.05/0.16
	Steel	3	6.16/0.36
VC40	CFRP	3	1.15/0.07
	Steel	3	4.31/0.22
VC60	CFRP	3	3.62/0.12
	Steel	3	5.72/0.37

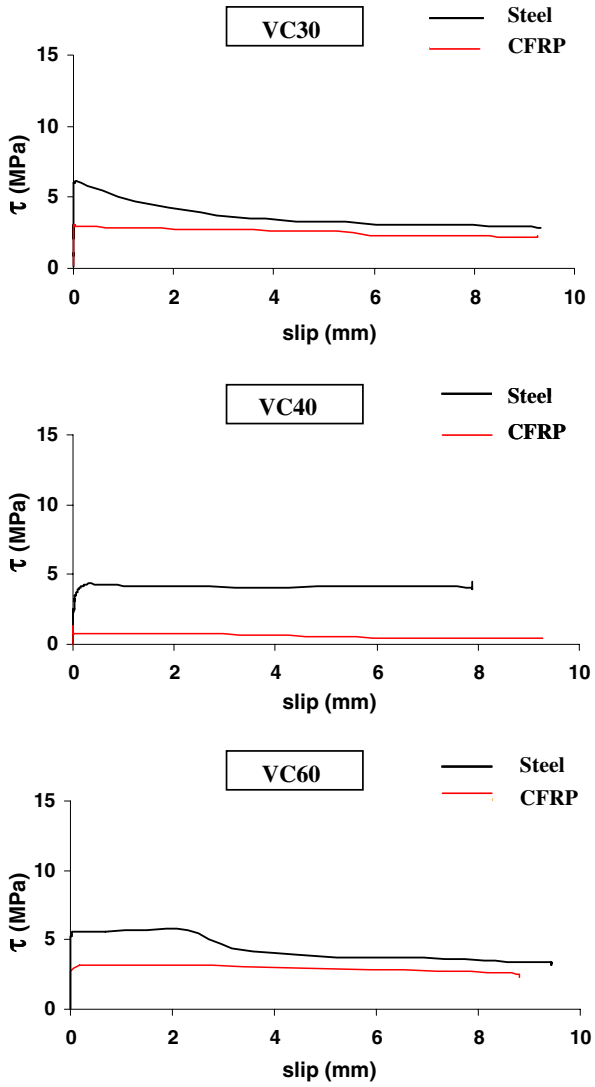

Fig. 9. Bond stress vs. slip typical curve of smooth CFRP rods and steel bars for three strengths of concrete.

The τ–s curves have different shapes in relation with the type of machining of the CFRP rods, both in the ascending and the softening parts. The softening branch represents the residual friction (Fig. 11).

The curves of the CFRP rod types 1 and 3 and the steel are very similar, whatever the bond length. All specimens,

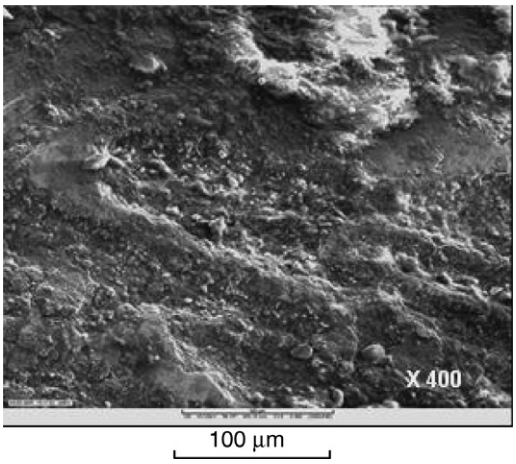

Fig. 10. Surface of steel bar.

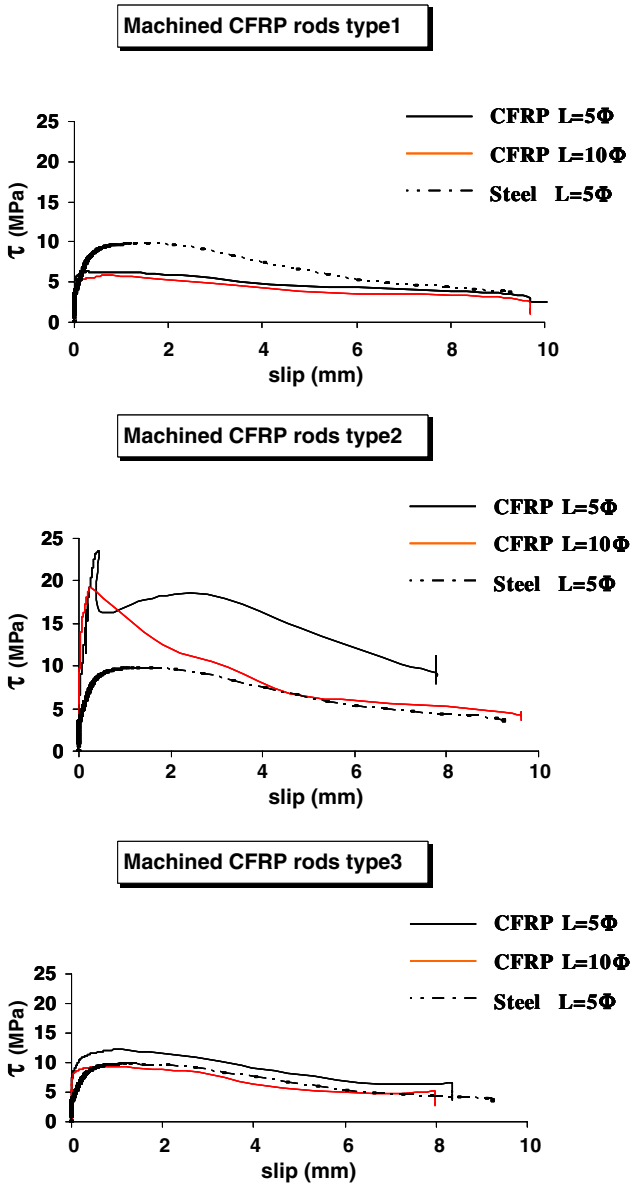

Fig. 11. Bond stress vs. slip typical curve of machined CFRP rods and steel bars.

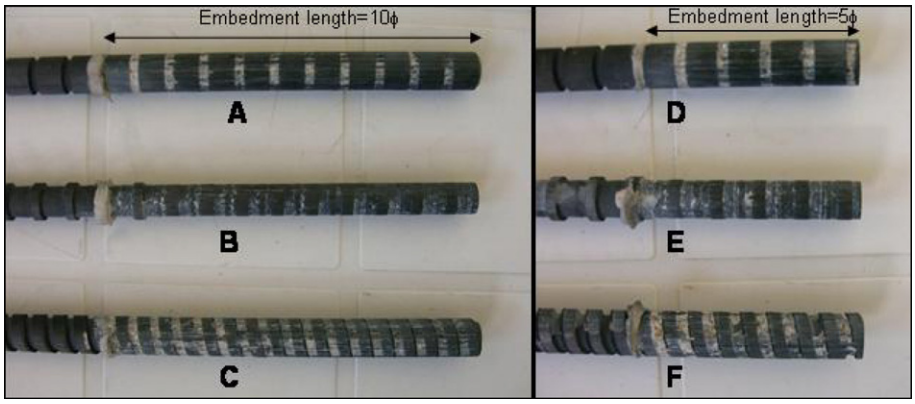

Fig. 12. A, B and C: machined CFRP rods types 1, 2 and 3, respectively $L = 10\varnothing$ after pull-out D, E and F: machined CFRP rods types 1, 2 and 3, respectively $L = 5\varnothing$ after pull-out.

Table 5
Summary of ultimate load, bond strength. and slip for sanded and machined rods and smooth steel bars (VC30 concrete), SD: standard deviation

FRP configuration surface	Ld	Number of samples	At maximum		Mode of failure	
			Load (N)	τ_u/SD (MPa)		
Machined type (1)	5∅	3	14.205	6.28/0.35	Pull-out	Shear off of concrete
	10∅	1	26.760	5.91		
Machined type (2)	5∅	3	45.804	24.3/1.41	Pull-out	Shear off of CFRP lugs
	10∅	1	72.610	19.26		
Machined type (3)	5∅	3	28.455	12.58/0.64	Pull-out	Shear off of concrete
	10∅	1	42.160	9.32		
Sanded type (1)	5∅	4	20.131	8.9/0.6	Pull-out	Pull-out of sand grain from resin layer
	10∅	1	40.500	8.95		
Sanded type (2)	5∅	4	33.499	14.81/0.39	Pull-out	Partial shear off of resin layer
	10∅	1	56.820	12.56		
Sanded type (3)	5∅	4	35.739	15.8/0.79	Pull-out	Shear off of resin layer
	10∅	1	50.400	11.14		
Ribbed steel	5∅	3	21.918	9.69/0.34	Pull-out	Shear off of concrete

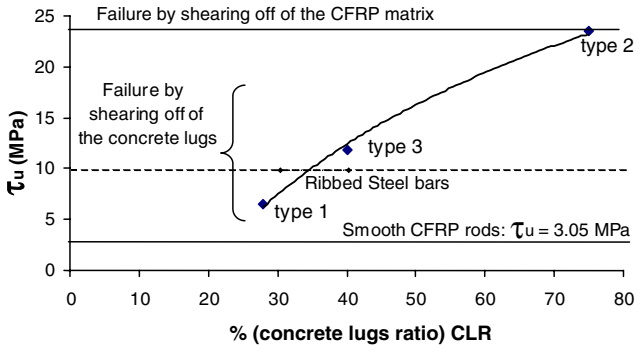

Fig. 13. Ultimate bond strength versus concrete lug ratio along 5∅ bond length.

types 1 and 3 and steel, failed by shearing off of the concrete lugs. The softening part is characterized by a decrease in the load to approximately 50% of the ultimate load.

However, for a constant bond length of 5ϕ, the ultimate bond strength τ_u obtained in these three cases were significantly different. Type 1 rod shows an ultimate bond strength approximately 46% lower than that of type 3 rod and approximately 32% lower than that of ribbed steel bars. This can be explained by the concrete lug ratio (CLR), defined as the concrete lug width in relation to the concrete and CFRP width (total bond length) (Fig. 2). For type 1 and type 3 rods, the CLRs are 25% and 40%, respectively. As shown in Fig. 13, increasing the CLR increases the ultimate bond strength of the rods. At the limit, if the CLR is large enough, rupture occurs by the shearing off of the CFRP lugs as in the case of the type 2 rod, with an ultimate bond strength more than twice that of the steel bars. In the case of the type 2 rod, after the ultimate bond strength is reached, the load drops instantaneously due to the failure of the rod matrix. In spite of this abrupt drop in the load, the residual friction (softening branch) remains equivalent to or greater than that for the

ribbed steel bar. The CLR of the steel depends on the shape of the lugs. It could be estimated to vary from 30% to 40% for the bar used in our study.

The bond strength of the machined rods is linked to the CLR. Fig. 13 shows that, in the case of the concrete used (VC30), a CLR of 35% is sufficient to ensure a bond strength equivalent to that of ribbed steel bar. But a better bond strength is obtained when failure occurs by the shearing off of the CFRP lugs.

An optimum CLR leading to a maximum pull-out load of the machined CFRP rods can be calculated from the experimental results. Assuming that the embedment length is 5∅ including 5 lugs with 1 mm height. The optimum CLR is reached if the shear strengths of the FRP lugs and the concrete lugs are equal (balanced failure): (concrete ultimate shear strength × CLR) = (CFRP matrix ultimate shear strength × (1 − CLR)).

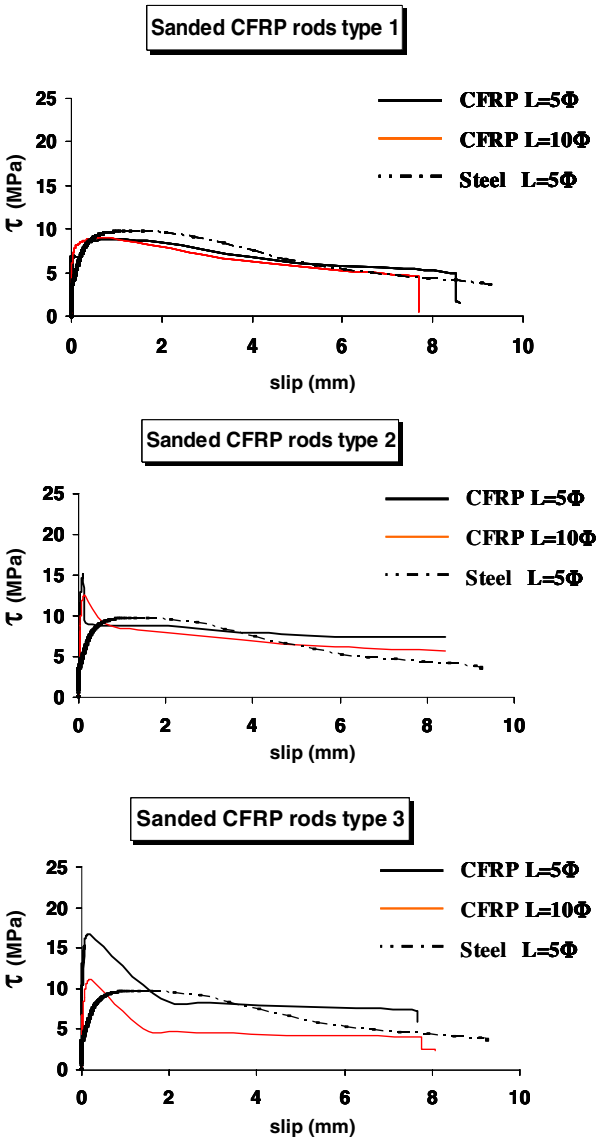

Fig. 14. Bond stress vs. slip typical curve of sanded CFRP rods and steel bars.

According to our experiments, the concrete ultimate shear strength (type 1 failure) is around 28.1 MPa (5 lugs of ($\pi \times 12 \times 2.8$) 105.5 mm^2 concrete surface failure due to shear stress) and the rod matrix ultimate shear strength (type 2 failure) is around 100.5 MPa (5 lugs of ($\pi \times 10 \times 2.8$) 87.9 mm^2 matrix surface failure due to shear stress). Then, the rod matrix ultimate shear strength is about (100.5/28.1) 3.6 times that of the concrete.

The calculation of these ultimate shear strengths is performed by dividing the ultimate pull-out load by the surface failure of concrete or matrix. The calculated CLR that ensures a failure of the rod matrix is 78%, which is almost the case for type 2 rods.

The ultimate shear strength calculated are far from those obtained using the Coulomb–Mohr theory (20% of the axial compression strength (7 MPa for the concrete)) because the failure mode involved is complex due to the combined compressive and shear stresses in the lugs.

Finally, for the three types of machined rod, the ultimate bond strength τ_u was always higher for 5∅ than for 10∅ embedment length. The decreases in τ_u were approximately 10%, 20% and 25%, respectively. This is due to the non-uniform distribution of the shear stresses [15,27].

4.2.3. Specimens reinforced with sanded rods

The experimental results obtained for the sanded CFRP rods with 5∅ and 10∅ embedment lengths in a VC30 concrete are shown in Fig. 14. As previously, only one representative curve for each configuration is reported in Fig. 14. Table 5 also gives the average ultimate load and the average ultimate bond strength obtained on the four specimens (in the case of 5∅ embedment length).

Results show that the ultimate bond strength of the sanded CFRP rods decreases with the reduction of the sand size. The difference between the bond strength of the sanded CFRP rod type 1 and the two other types (which are almost equivalent) is the most significant (up to 50% τ_u reduction) whatever the embedment length. For type 1 sanded rods, the failure occurs mostly by pull-out of the sand from the resin layer (Fig. 15). In this case, the shape of the τ–s curve (including the softening part) and the value of τ_u are similar to those of the ribbed steel bars. In contrast, type 3 sanded rods failed by slipping of the whole resin layer on the rod, whatever the embedment length. The same type of failure was observed on the type 2 sanded rods although a small part of the resin layer persisted on the rod, (Fig. 15). In conclusion, with small-grain sand (type 1), the bond strength and the residual friction of the CFRP rod with the concrete were equivalent to those of the ribbed steel bar. But, by increasing the size of the sand (types 2 and 3), the bond strength can be enhanced to reach twice that of the ribbed steel bar. In the latter cases, the shape of the τ–s curves is significantly different than the one of the ribbed steel bar. After the ultimate bond strength is reached, the load drops due to brittle failure, which was experimentally observed to occur between

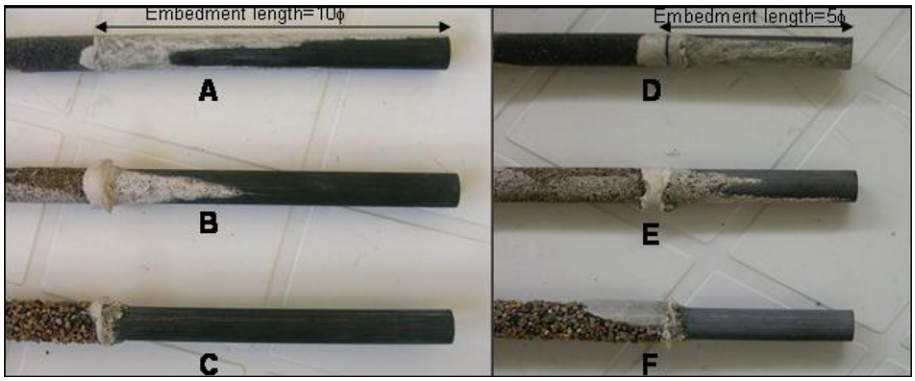

Fig. 15. A, B and C: sanded CFRP rods types 1, 2 and 3, respectively $L = 10\varnothing$ after pull-out; D, E and F: sanded CFRP rods types 1, 2 and 3, respectively $L = 5\varnothing$ after pull-out.

the resin layer and the rod. This τ–s curve is reminiscent of the one observed on the type 2 machined rod, where the pull-out occurred by failure of the rod's resin matrix. In terms of the softening branch, Fig. 14 shows that, in spite of this brittle drop in the load, the residual friction remains almost equivalent to or greater than in the case of ribbed steel bar.

As previously, the calculated ultimate bond strength τ_u is always higher for $5\varnothing$ than for $10\varnothing$ embedment length because of the non-uniform distribution of the shear stresses. This is clearly the case for the types 2 and 3 sanded rods [27,28].

4.2.4. Modeling the bond–slip constitutive relationship

It is necessary to ensure that the available models, elaborated for ribbed steel bars, are also valid to predict the bond stress–slip curves of the machined or sanded rods in concrete.

The differential equation that governs the bond problem [29] is obtained by considering:

- the equilibrium of the bar:
$$\frac{\pi\phi^2}{4}\,\mathrm{d}\sigma = \pi\phi\tau\,\mathrm{d}x \tag{3}$$
- a linear elastic behavior of the bar which, if the contribution of concrete in tension is neglected, is given by:
$$\sigma = E\varepsilon \cong E\frac{\mathrm{d}s}{\mathrm{d}x} \tag{4}$$
where E and ϕ are the elastic modulus and the diameter of the bar, respectively.

From Eqs. (3) and (4) the following differential equation is obtained:

$$\frac{\mathrm{d}^2 s}{\mathrm{d}x^2} - \frac{4}{E\phi}\tau(x) = 0 \tag{5}$$

The bond-slip behavior is analytically modeled with:

(1) An ascending branch for $s < s_m$ which is coincident with the first branch of the Eligehausen, Popov and Betero law (EPB) model [30]:
$$\tau(s) = \tau_u\left(\frac{s}{s_m}\right)^{\alpha} \tag{6}$$
where τ_u is the ultimate bond stress; s_m is the slip at ultimate bond stress; and α is a curve-fitting parameter influencing the shape of the bond–slip curve in the ascending branch and obtained by equating the area underneath the ascending branch of the experimental curve to the value:
$$A_\tau(0, s_m) = \int_0^{s_m} \tau_u\left(\frac{s}{s_m}\right)^{\alpha}\mathrm{d}s = \frac{\tau_u s_m}{1+\alpha} \tag{7}$$

(2) For $s > s_m$ the softening branch is given by:
$$\tau(s) = \tau_u + p(s - s_m) \quad \text{for } s_m \leqslant s \leqslant s_f \tag{8}$$
$$\tau(s) = \tau_f \quad \text{for } s \geqslant s_f \tag{9}$$
where p is the slope of the linear descending branch of the bond–slip curve and s_f is the slip value at the beginning of the frictional branch [16,20].

Table 6
Parameters in bond–slip relationships (bond length = $5\varnothing$)

FRP configuration surface	At maximum		τ_f (MPa)	α	P (MPa/mm)	Failure mode	
	τ_u (MPa)	S_m (mm)					
Machined type (1)	6.57	0.65	4.13	0.06	−0.54	Pull-out	Shear off of concrete
Machined type (2)	23.46	0.44	16.4	0.53	+428.7	Pull-out	Shear off of CFRP lugs
Machined type (3)	12.16	0.98	6.37	0.14	−1.09	Pull-out	Shear off of concrete
Sanded type (1)	8.82	0.97	5.55	0.12	−0.55	Pull-out	Pull-out of sand grain from resin layer
Sanded type (2)	15.24	0.11	7.95	0.28	−243	Pull-out	Partial shear off of resin layer
Sanded type (3)	16.79	0.17	8.04	0.15	−3.19	Pull-out	Shear off of resin layer

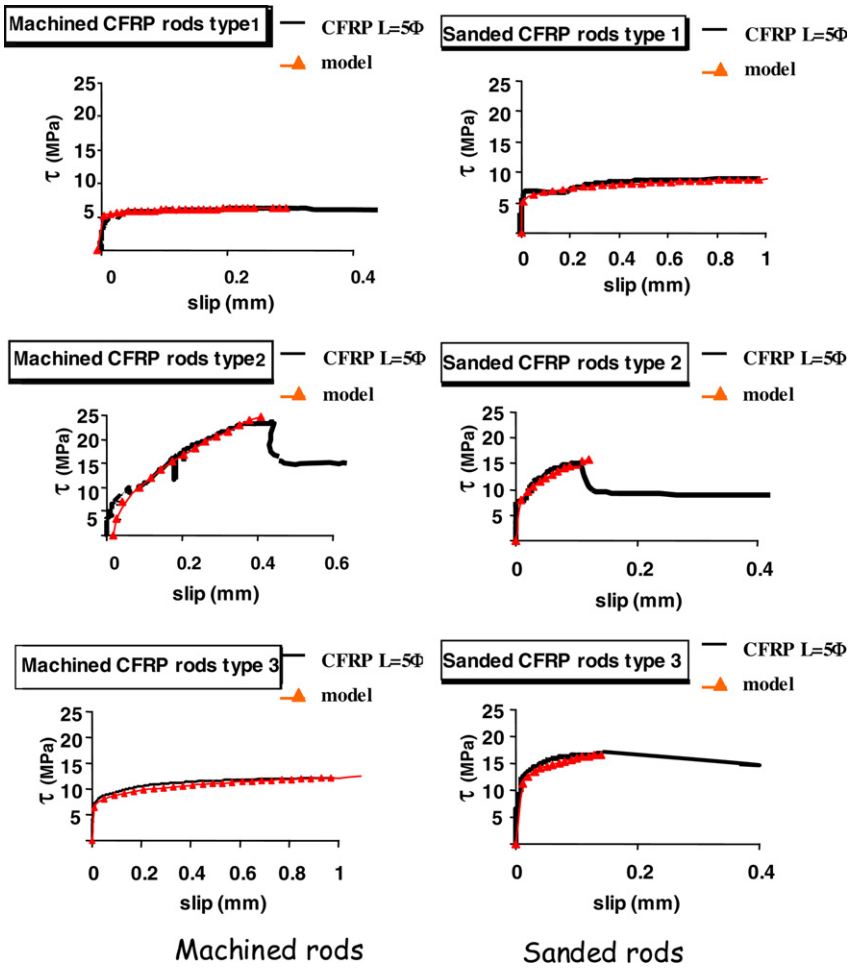

Fig. 16. Model prediction for ascending branch compared to experimental bond stress vs. slip for sanded and machined CFRP rods for 5∅ embedment length.

Table 6 gives the values of the unknown parameters calibrated by best fitting of experimental results obtained for the three types of machined CFRP rods and three types of sanded CFRP rods.

From these results we can make the following observations:

- For the type 2 machined CFRP rods and the types 2 and 3 sanded CFRP rods, the value of s_m is lower, indicating that the bond–slip curve is stiffer (ascending branch). We notice that the ultimate bond strength of type 2 machined CFRP rod and types 2 and 3 sanded CFRP rod is the highest.
- The absolute value of p for types 1 and 3 machined CFRP rods and type 1 sanded CFRP rods is lower (range 0.54–1.09), indicating a lower rate of decrease of the bond stress after s_m and before the frictional branch. For the type 2 machined CFRP rods and the types 2 and 3 sanded CFRP rods, the absolute value of p ranges from 3.19 to 428.7, indicating that the fall of the descending branch is more abrupt compared with the other types, due to the failure of the resin layer of the sanded rods types 2 and 3 and to the failure of the resin matrix of machined rod type 2.

A comparison between bonds calculated according to Eq. (6) for the ascending branch and the experimental results for all the CFRP rods with the 5∅ embedment length is shown in Fig. 16. It can be seen from these figures that the existing model elaborated for ribbed steel bars is also valid for both machined and sanded CFRP rods.

5. Conclusions

The experimental program aimed to investigate the possibility of using CFRP rods to strengthen concrete structural members. The following conclusions may be drawn.

CFRP, concrete and steel compatibility:

– X-ray diffractometry results for cement paste at the interface with CFRP rod show that the hydrates in contact with the carbon are the same as those formed in contact with steel, which tend to assume that the

interactions are similar to those when steel bars are used. Moreover, the CFRP rod is not porous to water and so does not influence the degree of hydration of the surrounding concrete.
– The elastic modulus of the CFRP rod is around 146 GPa. The difference with the elastic modulus of steel could be a compatibility problem when CFRP is used as a strengthening material for steel-reinforced structures.

Bond with concrete:

– The bond between smooth CFRP rods and concrete is significantly lower than the smooth steel bar and concrete bond. This is due to the low roughness of the smooth CFRP rods in comparison with the roughness of steel.
– It is possible to use a surface treatment to enhance the bond of the rods. Two types of surface treatment were applied: machining on a lathe with a grinding stone or sand coating with an epoxy resin and various sand grain sizes. Results show that, the ultimate bond strength of both machined and sanded rods can reach twice that of ribbed steel bars. Moreover, the residual friction between the CFRP rods and the concrete (softening branch) remains equal to or greater than that found for ribbed steel bar.

In regard to the experimental results, CFRP rods seem to be a good option for strengthening concrete structural members. The next stage of work concerns the strengthening by setting of CFRP rods in existing structures. The option selected is implementation by near-surface mounted (NSM) technique in the tension parts of the reinforced concrete elements. The CFRP rods are then placed in grooves using a mortar or an epoxy resin.

Authors believes that results concerning the bond properties could be generalized to any CFRP rods in the case of the surface sanding technique. Indeed, bond with concrete does not depend significantly on the rod material properties (matrix resin, carbon density, ...). Nevertheless, bond properties of machined rods could be influenced by the matrix resin shear strength and the carbon density of the rods.

Acknowledgement

The authors acknowledge the Freyssinet Company, France for its financial support.

References

[1] L'Hermite R, Bresson J. Béton armé d'armatures collées. In: Proceedings of the RILEM symposium on synthetic resins in building construction; 1967. p. 175–203.
[2] Bresson J. L'application du béton plaqué. Annales de l'ITBTP; 1971. p. 239.
[3] Raithby KD. External strengthening of concrete bridges with bonded steel plates. Suppl. Report 612. Transport and Road Research Laboratory; 1975.
[4] De Lorenzis L, Nanni A. Shear strengthening of reinforced concrete beams with near-surface mounted fiber-reinforced polymer rods. ACI Struct J 2001(January–February):60–8.
[5] De Lorenzis L, Rizzo A, La Tegola A. A modified pull-out test for bond of near-surface mounted FRP rods in concrete. Composites 2002;33:589–603.
[6] De Lorenzis L, Nanni A. Bond between near-surface mounted fiber-reinforced polymer rods and concrete in structural strengthening. ACI Struct J 2002(March–April):123–31.
[7] De Lorenzis L, Lundgren K, Rizzo A. Anchorage length of near-surface mounted fibre reinforced polymer bars for concrete strengthening experimental investigation and numerical modeling. ACI Struct J 2004(March–April):269–77.
[8] De Lorenzis L. Anchorage length of near-surface mounted fiber reinforced polymer bars for concrete strengthening – analytical modeling. ACI Struct J 2004(May–June):375–86.
[9] Novidis D, Pantazopoulou 1 SJ, Tentolouris E. Experimental study of bond of NSM-FRP reinforcement. Construct Build Mater 2006:1–11.
[10] Barboni M, Benedetti A, Nanni A. Carbon FRP strengthening of doubly curved precast PC shell. J Compos Construct 1997;1: 168–74.
[11] Emmons PH, Vaysburd AM, Thomas J. Strengthening concrete structures, part 2. Concr Int 1998:56–60.
[12] Midwater KR. Plate bonding carbon fiber and steel plates. Construct Repair 1997;11:5–8.
[13] Nanni A. Concrete repair with externally bonded FRP reinforcement: examples from Japan. Concr Int 1995;17:22–6.
[14] Bakis CE, Uppuluri VS, Nanni A, Boothby TE. Analysis of bonding mechanisms of smooth and lugged FRP rods embedded in concrete. Compos Sci Technol 1998;58:1307–19.
[15] Al-Zahrani MM, Al-Dulaijan SU, Nanni A, Bakis CE, Boothby TE. Evaluation of bond using FRP rods with axisymmetric deformations. Construct Build Mater 1999;13:299–309.
[16] Toutanji H, Deng Y. Deflection and crack-width prediction of concrete beams reinforced with glass FRP rods. Construct Build Mater 2003;17:69–74.
[17] Al-Zahrani MM, Al-Dulaijan SH. Annotated bibliography of bond behavior in FRP/concrete systems. Report CMTC-9501, Composite Manufacturing Technology Centre, The Pennsylvania State University, University Park, (PA) 16802, November; 1995. p. 72.
[18] Kocaoz S, Samaranayake VA, Nanni A. Tensile characterization of glass FRP bars. Compos, Part B 2005:127–34.
[19] Tighiouart B, Benmokrane B, Gao D. Investigation of bond in concrete member with fibre reinforced polymer (FRP) bars. Construct Build Mater 1998;12:453–62.
[20] Makitani E, Irisawa I, Nishiura N. Investigation of bond in concrete member with fibre reinforced polymer (FRP) bars. ACI SP-138; 1993. p. 315–31.
[21] Burgogne CJ. Should FRP be bonded to concrete? In: International symposium fibre-reinforced plastic reinforcement for concrete structures, ACI SP-138; 1993. p. 367–80.
[22] Al-Zahrani MM, Nanni A, Al-Dulaijan SU. Bakis CE. Bond of FRP to concrete in reinforcement rods with axisymmetic deformations. In: Proceedings of the 2nd international conference on advanced composite materials in bridges and structures. Montreal: M.M. El-Badry, August, 1996. p. 11–4.
[23] Al-Zahrani MM, Nanni A, Al-Dulaijan SU, Bakis CE. Bond of FRP to concrete. Proceedings of the 51st annual conference of the composites institute. New York: Society of the Plastics Industry; 1996. p. 3A1–8.
[24] Pecce M, Manfredi G, Realfonzo R, Cosenza E. Experimental and analytical evaluation of bond properties of GFRP bars. J Mater Civil Eng 2001(July–August):282–9.
[25] AFPC-AFREM Durabitlé Des Betons "Méthodes recommandées pour la mesure des grandeurs associées à la durabilité" Toulouse; 1997. p. 59–64.

[26] RILEM Essai portant sur l'adhérence des armatures du béton: essai par traction, Materials and Structures, (3) 15; 1970.
[27] Cosenza E, Manfredi G, Realfonzo R. Development length of FRP straight bars. Composites 2002;33:493–504.
[28] Benmokrane B, Zhang B, Chennouf A. Tensile properties and pullout behaviour of AFRP and CFRP rods for grouted anchor applications. Construct Build Mater 2000;14:157–70.
[29] Rehm G. Uber die Grundlagen des Verbundes Zwischen Stahl und Beton. Deutscher Ausschuss fur Stahlbeton, Helft; 1961. p. 138.
[30] Eligehausen R, Popov E, Bertero VV. Local bond stress–slip relationships of deformed bars under generalized excitations, Report No. 83/23, EERC, University of California-Berkeley, Berkeley (CA); 1983. p. 162.